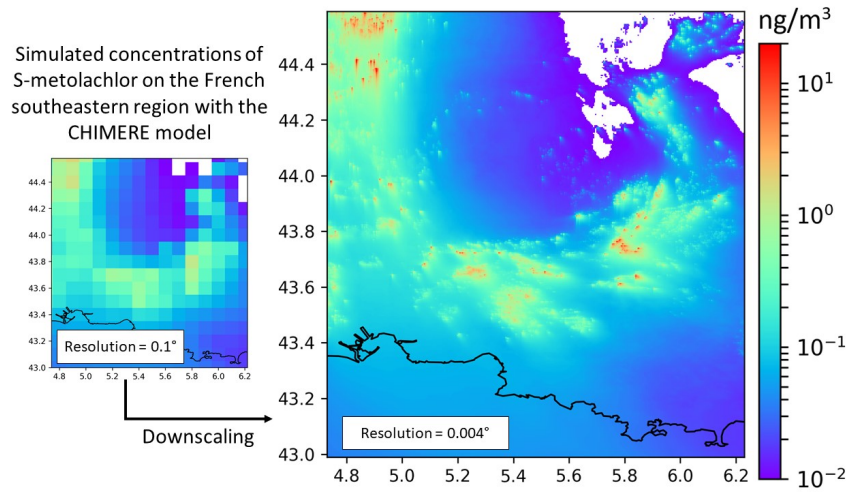


Graphical Abstract

An online downscaling method to simulate high resolution atmospheric concentrations of pesticides with the 3D chemistry-transport model CHIMERE: application and evaluation

Florian Couvidat,, Carole Bedos, Philippe Martin, Thomas Poméon, Etienne Quivet



An online downscaling method to simulate high resolution atmospheric concentrations of pesticides with the 3D chemistry-transport model CHIMERE: application and evaluation

Florian Couvidat,^{a,*}, Carole Bedos^b, Philippe Martin^c, Thomas Poméon^d, Etienne Quivet^e

^aINERIS, Institut National de l'Environnement Industriel et des Risques, Parc Technologique ALATA, Verneuil-en-Halatte, 60550, France

^bParis-Saclay Univ. INRAE AgroParisTech UMR ECOSYS 78850 Thiverval-Grignon France

^cUMR SADAPT AgroParisTech INRAE Paris-Saclay Univ. 78850 Thiverval-Grignon France

^dUS ODR INRAE 31326 Castanet-Tolosan France

^eAix Marseille Univ CNRS LCE Marseille France

Abstract

High resolution databases on atmospheric concentrations of pesticides are necessary in order to perform epidemiological studies but there is currently no modeling method to provide high resolution mapping of pesticides concentrations over a whole region. In this study, we propose an online downscaling method for CHIMERE to perform simulations at a sub-kilometer resolution. The main idea of this downscaling approach is to redistribute or interpolate some information simulated on the coarse grid to simulate the transport over a finer subgrid. The performance of the downscaling is analyzed by comparing the CHIMERE nested simulation results at 0.02° and CHIMERE simulation results downscaled from 0.1° to 0.02° .

By applying this method to S-metolachlor, we diagnosed an error generated by the downscaling of a few percents on both background and hotspot concentrations. The method was used to simulate concentrations over France at a resolution of 0.004° with a limited increase of the computational time. Based on these simulations, we estimated that around 3 000 inhabitants were exposed to concentrations of S-metolachlor above 10 ng/m^3 from April 15th to May 15th 2014.

Keywords: Pesticide, Air quality, Modelling, Downscaling

1. Introduction

Pesticides are chemical products widely used in agriculture for pest management and therefore to prevent yield losses. Because pesticides can be emitted into the atmosphere by the drift of spray droplet and by the volatilization from

*Corresponding author, email: florian.couvidat@ineris.fr

5 treated surfaces, pesticides can be present in the atmosphere. Numerous stud-
6 ies have confirmed the presence of pesticides in the atmosphere (e.g., studies of
7 Moussaoui et al. (2012); Coscollà et al. (2017) or Désert et al. (2018)) and their
8 possible health effects on residents (Cognez et al., 2019; Teyssere et al., 2020).
9 However, their ubiquity in the atmosphere raises numerous concerns on the ex-
10 position of the population as a whole and not only residents living in proximity
11 of crops where pesticide are applied.

12 Reliable estimates of pesticide exposure for the whole population are needed
13 in order to perform national-scale or regional-scale epidemiological studies. 3D
14 Chemical Transport Models (CTM) could be used to provide large scale maps of
15 pesticide concentrations. This type of models have been developed to simulate
16 the formation and transport of main pollutants (such as ozone and particulate
17 matter) by representing the physicochemical processes involved in their evolu-
18 tion (such as gas-phase chemistry of radicals and major compounds, particle
19 formation, gas/particle partitioning, deposition).

20 Recently, Couvidat et al. (2022) implemented in the CHIMERE CTM (Mailler
21 et al., 2017) a method to simulate the concentrations of pesticides and has shown
22 that CTMs could be applied to the mapping of atmospheric concentrations of
23 pesticides as long as the spatiotemporal distribution of pesticide applications can
24 be adequately estimated. In this method, the model estimates the emissions by
25 volatilization of pesticides from treated surfaces with a distinction between the
26 volatilization from the soil and vegetation compartments. The authors applied
27 the method to simulate the S-metolachlor and folpet atmospheric concentra-
28 tions over France and its southeastern region. However, CTM simulations are
29 generally performed at a low resolution (from a few kilometers to hundreds of
30 kilometers) due to the high computational cost. While these models could be
31 applied to estimate the background atmospheric concentrations, the hotspots
32 of concentrations may be missed due to the low resolution. One challenge of
33 applying CTM results for regional-scale epidemiological studies is therefore to
34 reach a sufficient resolution.

35 Several methods are used to map atmospheric pollutants at high resolution
36 based on CTM results. A general distinction can be made between the nesting
37 approach and the downscaling approach. The former approach (by nesting) is
38 used to run the model over a smaller geographical domain with higher resolutions
39 (using the larger domain as boundary conditions). Although this method is
40 suitable for simulating small regions, its use can be quickly limited by the CPU
41 time need to launch numerous time-consuming simulations over different nested domains to obtain high-resolution
42 mapping of concentrations over large areas.

43 The latter approach (downscaling) can be calculated by interpolation (bilinear,
44 kriging) from CTM outputs. However, in order to increase spatial accuracy
45 while maintaining correct performance scores, accurate emission proxies (e.g.
46 Bessagnet et al. (2023)) or a Gaussian dispersion model (Denby et al., 2020;
47 Hooyberghs et al., 2022) need to be used with such methods. Finally, thanks
48 to advances in machine learning and the increased availability of satellite data,
49 statistical regression approaches based on land use characteristics (Land Use
50 Regressions models) can offer promising spatial resolutions. However, temporal
51 resolution is often limited to daily time steps at best (e.g. Hough et al. (2021);
52 Shen et al. (2022)). LURs seem to have difficulty competing with CTMs in
53 terms of process dynamics.
54

55 The objective of the present study is to develop an online method (applied
56 directly inside the CHIMERE CTM and not on simulation results) in order to
57 downscale simulated concentrations from a coarse resolution to a sub-kilometer
58 resolution and to evaluate the performance of the downscaling. Instead of pro-
59 cessing simulation results, this method consists in redistributing or interpolating
60 fluxes calculated over the coarse grid onto a finer subgrid in order to compute the
61 atmospheric chemical transport of compounds over this subgrid. This method
62 aims therefore at reproducing the results that would be obtained by nesting
63 without solving again all the physicochemical processes in order to save CPU
64 time. To provide an illustration, the downscaling approach is applied to the sim-
65 ulation of S-metolachlor concentrations (the compound from the two pesticides
66 simulated by Couvidat et al. (2022) with the best comparison to measurements
67 performance).

68 The methodology for the downscaling is presented in the Method section.
69 Finally, the performance of the downscaling is evaluated by comparing the re-
70 sults of the France simulation downscaled to 0.02° with the simulation results
71 (without the downscaling) over four separate subdomains directly with a 0.02°
72 resolution. The gain on the computation time due to the downscaling is also
73 studied.

74 2. Method

75 Concentrations of S-metolachlor are simulated over France from mid April
76 to mid May 2014 (application period of S-metolachlor) with a resolution of 0.1°
77 and are downscaled either to 0.02° or to 0.004° . As simulations at the 0.004°
78 resolution is too time consuming even over small spatial domains, the evaluation
79 of the downscaling approach is performed only for the 0.02° resolution on several
80 sub-domains.

81 Following Couvidat et al. (2022), the contribution of emission by spray-drift
82 during application to atmospheric concentration was assumed negligible because
83 of the resolution of the model. Indeed, due to the high diameter of spray-drift
84 droplets and their low lifetime in the atmosphere, a resolution of a few meters
85 would be needed to represent adequately their atmospheric transport. There-
86 fore, the current downscaling method only aims at representing pesticide con-
87 centrations due to emissions by volatilization. Nonetheless, the model considers
88 that spray-drift droplets are instantaneously deposited into the cell where they
89 are emitted and can contribute to subsequent emissions by volatilization.

90 2.1. Presentation of the pesticide version of CHIMERE

91 In order to estimate the atmospheric concentrations of pesticides, the CHIMERE
92 model computes the transport of compounds over a grid covering the studied
93 domain by accounting for advection and vertical diffusion. The vertical grid is
94 discretized into several vertical layers (9 layers in Couvidat et al. (2022) ranging
95 from 30 m to more than 5 000 m). The model uses a soil/vegetation/atmosphere
96 exchange module to compute the emissions by volatilization from treated sur-
97 faces. It is based on the approaches of Couvidat and Bessagnet (2021) and
98 Lichiheb et al. (2016) for the volatilization from the soil and leaves, respec-
99 tively.

100 This exchange module uses a resistance scheme and parameterizations to
101 consider the multiphase partitioning and diffusion in the soil compartment as

102 well as lifetime of the compounds in the different compartments. The model
103 also accounts for:

- 104 • The atmospheric degradation of pesticides by the OH radical (the model
105 can also account for direct photolysis and degradation by O₃ and NO₃
106 radicals if experimental data on reaction constants are available).
- 107 • The gas-particle partitioning of semivolatile pesticides between the gas
108 and the particle phases estimated with the Secondary Organic Aerosol
109 Processor model (Couvidat and Sartelet, 2015).
- 110 • The wet deposition (both by in-cloud and below-cloud scavenging) of gases
111 (based on Henry’s law constants) and the wet and dry deposition of par-
112 ticles.

113 In order to use the model, the spatiotemporal distribution of pesticide ap-
114 plications have to be estimated to compute the emissions by volatilization. In
115 Couvidat et al. (2022), the spatial distribution was given by the French BNVD-
116 S (“Banque Nationale des Ventes de produits phytopharmaceutiques par les
117 Distributeurs agréés - Spatialisée”) database (Martin et al., 2023) that uses
118 mandatory register on pesticide sales to estimate the spatialized usage of pesti-
119 cides over parcels. The temporal distribution was estimated based on enquiries
120 on agricultural practices over the southeastern region of France.

121 2.2. The online downscaling method

122 The online downscaling method consists in dividing the CHIMERE grid
123 into a subgrid with a finer resolution and in determining the necessary variables
124 for the computation of concentrations over the subgrid. Emissions rates over
125 the subgrid are determined by redistribution (the amount of emitted pesticides
126 onto a cell is redistributed on the different subcells). Other variable values
127 (meteorological parameters, deposition kinetics, chemical destruction kinetics)
128 are determined by an horizontal bilinear interpolation (interpolation between
129 the four closest cell center of the CHIMERE coarse grid). With this method,
130 concentrations can be efficiently computed without representing explicitly some
131 time consuming processes (such as the transport of all the model, gas-phase
132 chemistry, pesticide volatilization, gas-particle partitioning) over the subgrid .
133 The fraction of the different landuse categories inside each sub-cells is calculated
134 in order to determine the appropriate vertical mixing and deposition over the
135 subgrid.

In CHIMERE, concentrations at each cell of the grid are computed with a
semi-implicit numerical method in order to solve the following equation:

$$\frac{\partial C_{t,X,Y,Z}}{\partial t} = Prod_{t,X,Y,Z} - Loss_{t,X,Y,Z} \times C_{t,X,Y,Z} \quad (1)$$

136 With t,X,Y and Z the cell indexes for time, longitude, latitude, and altitude.
137 $Prod_{t,X,Y,Z}$ is the production rate of C in cell X,Y,Z (due to emissions or trans-
138 port of the compound into the cell) and $Loss_{t,X,Y,Z}$ is the loss kinetics of C in
139 cell X,Y,Z (due to chemical degradation, transport, and deposition).

140 In CHIMERE, a sectional approach is used where particles are separated
141 into N_{bins} (number prescribed by the user) bins according to their diameter. As
142 pesticides are semi-volatile compounds existing in both the gaseous and particle

143 phases, each pesticide is represented by $N_{bins}+1$ CHIMERE species (for the
144 N_{bin} size diameter bins and the gas phase fraction).

In the downscaling method, developed in this study, each cell of the CHIMERE simulation grid is divided into $N_{red} \times N_{red}$ sub-cells (N_{red} representing an integer number by which the resolution is reduced). The method consists in estimating the production rate $Prod_{t,X,Y,Z}$ and kinetics of loss $Loss_{t,X,Y,Z}$ over the sub-grid by redistributing or interpolating the rates over a finer grid in order to calculate the concentrations at a finer resolution. Eq. 1 is adapted to simulate the evolution of the concentrations on the finer grid such as:

$$\frac{\partial C_{t,X,Y,Z}^{sub,x,y}}{\partial t} = Prod_{t,X,Y,Z}^{sub,x,y} - Loss_{t,X,Y,Z}^{sub,x,y} \times C_{t,X,Y,Z}^{sub,x,y} \quad (2)$$

145 where x,y represent the longitudinal and latitudinal indexes of the sub-cell inside
146 the cell X,Y,Z. $Prod_{t,X,Y,Z}^{sub,x,y}$ and $Loss_{t,X,Y,Z}^{sub,x,y}$ represent the production rate and
147 loss kinetics of the sub-cell x,y inside cell X,Y,Z, respectively.

148 Moreover, in the downscaling approach, only one new model species (instead
149 of the $N_{bins}+1$ CHIMERE species) representing both the gas and particle phases
150 is transported on the CHIMERE subgrid. The total loss kinetics is determined
151 by ponderating the loss kinetics for the gas-phase and each of the particle bins
152 accounting for chemical degradation and deposition. More details are provided
153 in sections 2.2.1 to 2.2.3.

154 By simulating a limited number of CHIMERE species (instead of a hundred
155 of CHIMERE species) on the subgrid and by avoiding the computation of some
156 Central Processing Unit (CPU) consuming processes (computation of pesticide
157 volatilization and of the gas-particle partitioning), concentrations of pesticides
158 on a subgrid can be computed with limited CPU time.

$Prod_{t,X,Y,Z}^{sub,x,y}$ and $Loss_{t,X,Y,Z}^{sub,x,y}$ are decomposed as follow:

$$Prod_{t,X,Y,Z}^{sub,x,y} = Emissions_{t,X,Y,Z}^{sub,x,y} + ProdHTrans_{t,X,Y,Z}^{sub,x,y} + ProdVTrans_{t,X,Y,Z}^{sub,x,y} \quad (3)$$

$$Loss_{t,X,Y,Z}^{sub,x,y} = WetDep_{t,X,Y,Z}^{sub,x,y} + DryDep_{t,X,Y,Z}^{sub,x,y} + ChemLoss_{t,X,Y,Z}^{sub,x,y} + LossHTrans_{t,X,Y,Z}^{sub,x,y} + LossVTrans_{t,X,Y,Z}^{sub,x,y} \quad (4)$$

159 with $Emissions_{t,X,Y,Z}^{sub,x,y}$ the emission rate on the subgrid, $ProdHTrans_{t,X,Y,Z}^{sub,x,y}$
160 the production rate due to horizontal transport on the subgrid, $ProdVTrans_{t,X,Y,Z}^{sub,x,y}$
161 the production rate due to vertical transport on the subgrid, $DryDep_{t,X,Y,Z}^{sub,x,y}$
162 the dry deposition kinetics on the subgrid, $WetDep_{t,X,Y,Z}^{sub,x,y}$ the dry deposition
163 kinetics on the subgrid, $ChemLoss_{t,X,Y,Z}^{sub,x,y}$ the chemical degradation kinetics on
164 the subgrid, $LossHTrans_{t,X,Y,Z}^{sub,x,y}$ the loss kinetics due to horizontal transport on
165 the subgrid and $LossVTrans_{t,X,Y,Z}^{sub,x,y}$ the loss kinetics due to vertical transport
166 on the subgrid. $DryDep_{t,X,Y,Z}^{sub,x,y}$ and $Emissions_{t,X,Y,Z}^{sub,x,y}$ are equal to zero for alti-
167 tudes above the ground level (no dry deposition and no emission of pesticides).

168 Currently, concentrations of pesticides entering the French domain are as-
169 sumed to be null due to the lack of information on pesticide usages at the Eu-
170 ropean scale (that would be necessary to perform a simulation at the European
171 scale and obtain appropriate boundary conditions).

172 *2.2.1. Dry deposition*

173 In CHIMERE, the deposition kinetics is calculated as the function of the
174 deposition velocities (with different parameterizations for gases and particles)
175 and the landuse.

176 In each cell of the coarse domain, deposition velocities are computed for each
177 landuse categories (even if this category is absent from the cell) by computing
178 a vertical wind profile with the roughness length of the considered landuse. For
179 each landuse category, the deposition velocities on the subgrid are interpolated
180 and are combined to the fraction of the landuse category in the cell of the
181 subgrid.

The apparent deposition kinetics $DryDep_{t,x,y,landuse}$ for a particular landuse
of the grid is calculated as a function of the loss kinetics of gaseous and particle
compounds such as:

$$DryDep_{t,x,y,landuse} = \sum_i f_i DryDep_{t,x,y,landuse,i} \quad (5)$$

182 with i the index for the considered pesticide of the gas-phase CHIMERE species
183 ($i=1$) and for the particle species for each of the bins ($i=2$ to $i=N_{bins}+1$), f_i the
184 fraction of CHIMERE species to the total concentration of the pesticide (gas
185 + particle) and $DryDep_{t,x,y,landuse,i}$ the loss kinetics of i due to dry deposition
186 for a specific land use.

The loss kinetics due to dry deposition on the sub-cell is constructed by
combining the land use on the sub-cell and the interpolated apparent deposition
kinetics for specific land use.

$$DryDep_{t,X,Y,Z=0}^{sub,x,y} = \sum_{landuse} L_{x,y,landuse}^{sub,x,y} Bilinear(DryDep) \quad (6)$$

187 with $Bilinear$ the bi-linear interpolation function and $L_{x,y,landuse}^{sub,x,y}$ the surface
188 ratio of the considered land use in the sub-cell.

189 *2.2.2. Wet deposition*

The loss kinetics due to wet deposition is obtained by interpolating the
apparent loss kinetics due to wet deposition of total (gas + particles) pesticides
such as:

$$WetDep_{t,X,Y,Z}^{sub,x,y} = Bilinear\left(\sum_i f_i WetDep\right) \quad (7)$$

190 With $WetDep_{t,X,Y,Z,i}$ the loss kinetics due to wet deposition of i (i being the
191 index for the pesticides either in the gas-phase or one of the particle phase)

192 *2.2.3. Chemical degradation*

Similarly to Eq.7, $ChemLoss_{t,X,Y,Z}^{sub,x,y}$ is calculated by interpolating the appar-
ent loss kinetics due to chemical degradation of total (gas + particles) pesticides
such as:

$$ChemLoss_{t,X,Y,Z}^{sub,x,y} = Bilinear\left(\sum_i f_i ChemLoss\right) \quad (8)$$

193 With $ChemLoss_{t,X,Y,Z,i}$ the loss kinetics over the coarse grid due to chemical
194 degradation of i (i being the index for the pesticides either in the gas-phase or

195 in one of the particle bins). As in this study, no heterogeneous degradation of
 196 pesticides is taken into account, $ChemLoss_{t,X,Y,Z,i} = 0$ for particles.

197 This interpolation is based on the assumption that the chemical degradation
 198 of pesticides is linear and that the concentrations of oxidants (only the OH
 199 radical in the case of S-metolachlor) can be interpolated. The impact of these
 200 assumptions is probably low except in areas with very strong local emissions of
 201 nitrogen oxides.

202 2.2.4. Emissions

203 The atmospheric emissions fluxes are computed with the exchange air/soil/plant
 204 cover exchange module with emissions being calculated by volatilization from
 205 the soil or the plant cover.

206 Two types of emissions are distinguished:

- 207 • Emissions from treated crops. In this case, the calculated mass of pesticide
 208 emitted over a cell is redistributed over the different sub-cells according
 209 to the applicated amounts given by the BNVD-S on the sub-cells
- 210 • Re-emissions (emissions by re-volatilization of pesticides deposited on non-
 211 treated surfaces). In this case, the re-distribution of emissions fluxes is
 212 calculated as a function of the accumulated amount of pesticides at the
 213 surface $Accum_{t,X,Y}^{sub,x,y}$ (due to dry deposition on the first atmospheric verti-
 214 cal level and the cumulated wet deposition on all vertical layer) calculated
 215 with the following equation:

$$\begin{aligned}
 Accum_{t,X,Y}^{sub,x,y} &= \sum_Z (WetDep_{t,X,Y,Z}^{sub,x,y} C_{t,X,Y,Z}^{sub,x,y} \times \Delta H_Z) \\
 &+ DryDep_{t,X,Y,Z=0}^{sub,x,y} C_{t,X,Y,Z=0}^{sub,x,y} * \Delta H_{Z=0} - Accum_{t,X,Y}^{sub,x,y} k_{deg} \quad (9)
 \end{aligned}$$

216 with k_{deg} the degradation kinetics computed with the lifetime of com-
 217 pounds within the soil and ΔH_Z the thickness of the vertical layer.

218 2.2.5. Transport

219 The horizontal transport on the subgrid is solved with the same algorithm
 220 than the transport on the coarse grid. The necessary parameter (e.g., wind
 221 velocities) are downscaled by bilinear-interpolation.

222 In CHIMERE, the vertical transport is represented with the K-theory based
 223 on the K_z parameter calculated for each landuse categories. The vertical trans-
 224 port production rate and loss kinetics on the subgrid are computed for a level
 225 Z as a function of the K_z parameter on the interpolated on the subgrid and the
 226 concentrations on the level above ($Z+1$) and underneath ($Z-1$). It should be
 227 noted that following the treatment of deposition velocity the K_z explained in
 228 section 2.2.1, the K_z is calculated and interpolated for each landuse categories.
 229 The resulting K_z on the subgrid therefore accounts for the landuse.

230 In order to limit the number of cells, we added the possibility to simulate the
 231 vertical transport on $N_{lev,sub}$ vertical levels (inferior or equal to N_{lev} the number
 232 of vertical level of the coarse level). In that case, the model used interpolated
 233 concentrations from the coarse above $N_{lev,sub}$ to compute the vertical transport
 234 rate. The effect of $N_{lev,sub}$ on the results are discussed in section 3.3.

235 *2.3. Evaluation of the downscaling method*

236 The performance of the downscaling method to simulate high-resolution con-
 237 centrations of S-metolachlor is evaluated by comparing to CHIMERE simulation
 238 results obtained by nesting at the same resolution (0.02°). In that order, the
 239 results of a $0.1^\circ \times 0.1^\circ$ simulation downscaled to $0.02^\circ \times 0.02^\circ$ are compared
 240 to CHIMERE simulations directly at 0.02° over four nested domains. Indeed,
 241 it would not have been possible to perform simulations for a domain covering
 242 the whole France with a $0.02^\circ \times 0.02^\circ$ resolution (due to an important com-
 243 putation time). Simulations were performed over the four nested sub-domains
 244 illustrated in Fig. 1: NW (part of Northwestern France), NE (part of Northeast-
 245 ern France), SW (part of Southwestern France), and SE (part of Southeastern
 246 France). The SE subdomain corresponds to the French "Provence-Alpes-Côte
 247 d'Azur" subdomain studied by Couvidat et al. (2022). These four sub-domains
 248 were selected to cover the different situations encountered at the national scales
 249 (areas with high and low emissions, different climate conditions).

250 The results of a simulation over France at $0.1^\circ \times 0.1^\circ$ are used to determine
 251 the boundary conditions over the four subdomains for all pollutants except for
 252 S-metolachlor. In order to remove the influence of boundary conditions on the
 253 analysis, the results from the downscaled simulation at $0.02^\circ \times 0.02^\circ$ (with
 254 $N_{lev,sub}=N_{lev}$) were used as boundary conditions on the four subdomains (air
 255 masses entering the four subdomains have therefore the same concentrations
 256 than the downscaled simulation at 0.02°).

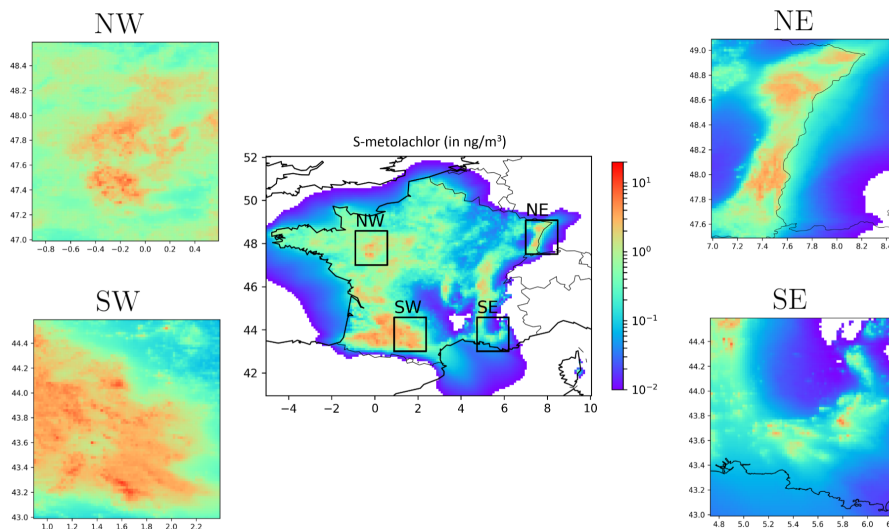


Figure 1: Simulated coarse concentrations of S-metolachlor (in ng/m^3) over France by CHIMERE at the 0.1° resolution (center) and on four nested sub-domains (in the four corners) at a resolution of 0.02° .

257 Several metrics are computed in order to evaluate the performance of the
 258 downscaling.

- 259 • The correlation coefficient R^2
- 260 • The Mean Normalized Bias (MNB): average of the bias (in %) between
 261 the downscaled simulation and the reference simulation at 0.02° .

- 262 • The Mean Normalized Error (MNE): average of the error (in %) between
263 the downscaled simulation and the reference simulation at 0.02° .
- 264 • The Mean Normalized Bias computed for the 1% highest values (1%MNB)
- 265 • The Mean Normalized Error for the 1% highest values (1%MNE)

266 The last two metrics provide information on the ability to reproduce the simu-
267 lated hotspots of pesticide concentrations in the 0.02° simulations.

268 *2.4. Simulation configuration*

269 The simulation configuration of Couvidat et al. (2022) was reproduced: an-
270 thropogenic emissions of gases and particles were taken from the European
271 Monitoring and Evaluation Programme (EMEP) inventory (Vestreng, 2003) for
272 the year 2014 and meteorology was taken from the operational analysis of the
273 Integrated Forecasting System (IFS) model of the European Centre for Medium-
274 Range Weather Forecasts (ECMWF). Nine vertical levels up to 500 hPa were
275 used. The thickness of the first layer is around 30 m.

276 Concentrations of S-metolachlor are simulated from 2014-04-15 (beginning of
277 the application period for S-metolachlor determined by Couvidat et al. (2022))
278 to 2014-05-15 (end of the application period).

279 **3. Results**

280 *3.1. Downscaling results*

281 Concentrations downscaled at 0.004° are shown in Fig. 2 and can be com-
282 pared to the simulation results at 0.1° in Fig. 1. Similar pattern is found at
283 the national scale with the same areas with high concentrations (southwest-
284 ern France, the Rhône valley, several areas in western France, frontier between
285 France and Germany) indicating that the model is able to simulate the back-
286 ground concentrations even at a low resolution.

287 The interest in downscaling the concentrations can be seen by zooming on
288 the results on the different sub-domains. Fig. 3 shows the maps of coarse con-
289 centrations at 0.1° and of downscaled concentrations at 0.02° . Maps at down-
290 scaled concentrations at 0.004° can also be found in Supplementary Materials
291 in figures S1 to S4. With a 0.1° resolution, the maps of concentrations are
292 pixelated and hotspots of concentrations cannot be reproduced. The evolution
293 of concentrations in the vicinity of areas with high emissions may not be well
294 reproduced. When downscaled at a higher resolution, the hotspots of concen-
295 trations appear more and more clearly while the overall background pattern is
296 unchanged. While the simulated average concentrations over France is around
297 0.2 ng/m^3 for all the coarse and downscaled simulations, the simulated maxi-
298 mum concentrations changed significantly: 5.3 ng/m^3 for the coarse simulation
299 at 0.1° , 14.5 ng/m^3 for the downscaled simulation at 0.02° and 116 ng/m^3
300 for the downscaled simulation at 0.004° . By combining these simulation results to
301 the French population database (Letinois, 2015), we estimated that a small part
302 of the population (around 3 000 inhabitants, 0.005% of the French population)
303 was exposed to concentrations of S-metolachlor above 10 ng/m^3 from April 15th
304 to May 15th 2014.

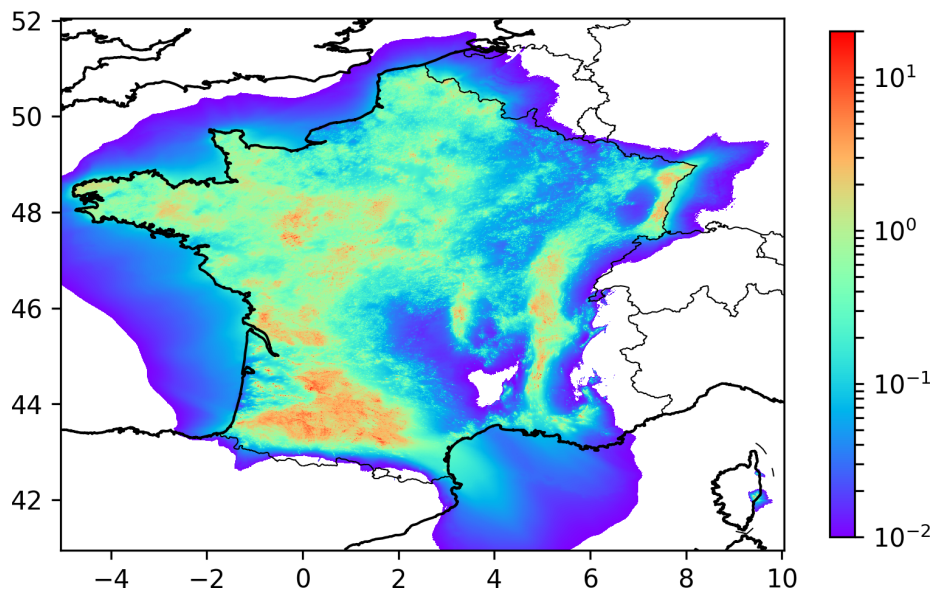


Figure 2: Simulations concentrations by CHIMERE (in ng/m^3) of S-metolachlor downscaled to a resolution of 0.004° . $N_{lev,sub}$ is chosen equal to N_{lev} .

3.2. Performance of the downscaling method

The performance of the downscaling method (illustrated by Fig. 4) is analyzed by computing R^2 , MNB, MNE, 1%MNB, 1%MNE between the CHIMERE results at 0.02° (not downscaled) and the CHIMERE results at 0.1° downscaled to 0.02° over the four sub-domains. These metrics are shown in Table B1 in Supplementary Materials for the different subdomains and for different value of $N_{lev,sub}$. The metrics are also shown between the coarse simulation at 0.1° and the simulation at 0.02° .

The coarse simulation is characterized by a large MNE of 25% over all domains (and varying from 18.1% to 35.2% over each sub-domains) and on average concentrations tend to be overestimated (MNB=11%). However, the highest concentrations are strongly underestimated by the coarse simulation (MNB=-43.1%).

The downscaling method managed to reproduce concentrations with a low bias compared to the coarse simulation as 90% of the simulated values have a bias between -14% and 11% for the downscaled simulation at 0.02° against a bias between -32% and 82% in the coarse simulation. When applying the downscaling, the correlation coefficient is increased significantly and reaches near unity ($R^2=0.99$, $R^2=0.9$ for the coarse simulation) especially for the SW domain where the R^2 is increased from 0.62 for the coarse simulation to 0.99 for the downscaled simulation (with $N_{lev,sub}=9$). MNE is also significantly reduced from 43.1% to 6.2% (with $N_{lev,sub}=9$). While the concentrations tend to be overestimated by the coarse simulations, the concentrations seems to be underestimated by the downscaling method but at a low extent (MFB=-2.6% over the four subdomains and reaching -4.6% for the SW subdomain). The downscaling approach managed to capture the highest values as the 1%MNB is decreased from -43.1% to -2.0% with a 1%MNE (6.1%) close to the average MNE.

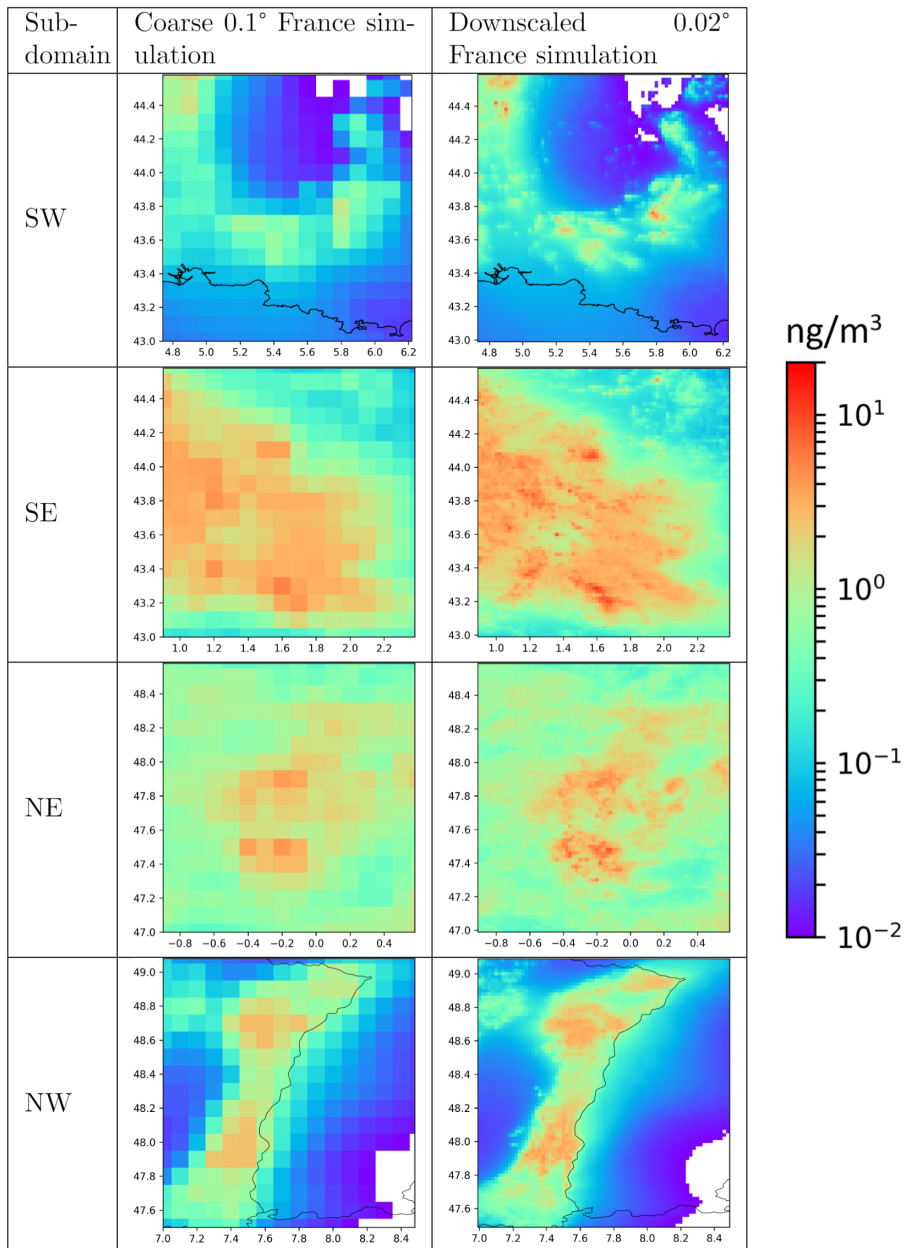


Figure 3: Maps of coarse simulated concentrations of S-metolachlor at the 0.1° resolution and of the downscaled concentrations at 0.02° (in ng/m³). $N_{lev,sub}$ is chosen equal to N_{lev} .

332 3.3. Computational time

333 The potential increase in computational time due to the downscaling ap-
 334 proach has to be assessed. As CPU time can be an important limitation for
 335 the use of CTM, it is important to diagnose the impact of the downscaling
 336 method on CPU time. Table 1 shows the CPU time increase under different
 337 configurations (different downscaled resolution and different value of $N_{lev,sub}$).

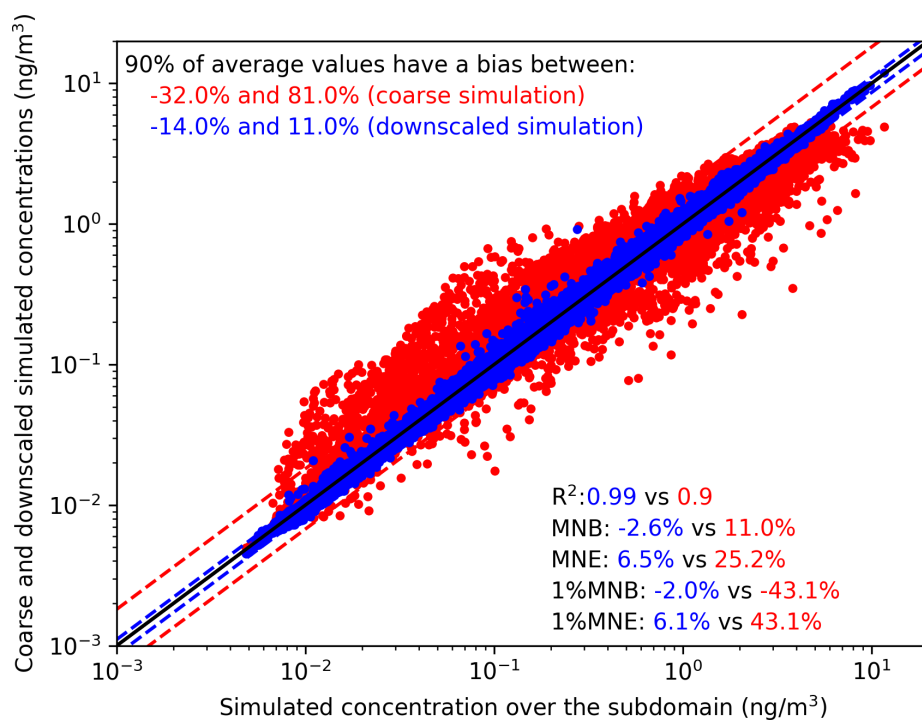


Figure 4: Distributions of the concentrations (in ng/m³) on the coarse domain (0.1° in red) and of the downscaled concentrations (0.02° in blue) as a function of the concentrations simulated on the 4 subdomains. The dashed lines provide the 90% interval including 90% of the simulations values with the lowest bias.

338 Downscaling the 0.1° results to a 0.02° resolution leads to an increase of CPU
 339 time of only 7% while launching CHIMERE directly at the a resolution of 0.02°
 340 would result in a CPU time increase close to a factor 125 (a factor 5×5 to de-
 341 crease the resolution of the horizontal grid combined to a factor 5 on temporal
 342 resolution in order to respect the Courant-Friedrich-Levy condition). The CPU
 343 time needed to run the downscaling approach is also much lower than the CPU
 344 time needed to perform simulations over the four nested sub-domains (increase
 345 of CPU time by a factor 3.79).

346 While the CPU time increase is modest for a downscaling to a 0.02° resolu-
 347 tion, it may lead to an important increase of CPU time to downscale to a 0.004°
 348 resolution (increase by a factor 9.16 with $N_{lev,sub}=9$). It should be noted that
 349 downscaling several pesticide at the same time may result in even greater CPU
 350 time. One possible way to limit the CPU time is to limit the number of vertical
 351 layer on the subgrid $N_{lev,sub}$. According to Table B1, using $N_{lev,sub}=3$ (3 layers
 352 covering an altitude around 250 m) may consist in a good compromise as the
 353 performance (MNE=7.9%, 1%MNE=6.6%) is similar to the performance with
 354 $N_{lev,sub}=9$ (MNE=6.5%, 1%MNE=6.1%).

Configuration	Relative computation time
France simulation at 0.1°	1
France simulation at 0.02°	125
France simulation at 0.1° + simulation on the four nested sub-domains	3.79
France simulation at 0.1° downscaled to 0.02° ($N_{lev,sub}=1$)	1.03
France simulation at 0.1° downscaled to 0.02° ($N_{lev,sub}=9$)	1.07
France simulation at 0.1° downscaled to 0.004° ($N_{lev,sub}=1$)	1.63
France simulation at 0.1° downscaled to 0.004° ($N_{lev,sub}=9$)	9.16

Table 1: Relative computational time compared to the France simulation at a resolution of 0.1° . The number corresponds to a downscaling method applied only on a single pesticide (S-metolachlor).

355 3.4. Comparison with measurements

356 Atmospheric measurement data of pesticides are scarce. However, since
 357 2011, the French Regional Networks for Air Quality compiled the atmospheric
 358 concentrations of pesticides in the PhytAtmo database. It aggregates about
 359 7,000 samples at 176 sites throughout mainland France and overseas for 321
 360 active substances sought (AtmoFrance, 2019). S-metolachlor was measured at
 361 24 stations in 2014, and at 91 stations between 2015 and 2020. However, the
 362 temporal coverage of these measurements are often partial and occur generally
 363 during a few days over the month.

364 According to this database, while the stations are not necessarily located
 365 near hotspots, concentrations of S-metolachlor can exceed 10 ng/m^3 in coherence
 366 with our simulation results showing hotspots above 10 ng/m^3 . Since 2014,

367 concentrations above 10 ng/m^3 and up to 51 ng/m^3 where detected 12 times at
368 3 different stations (for around 32 000 samples above the detection limit).

369 High S-metolachlor concentrations (around 14 ng/m^3) were measured at the
370 Ohnenheim station. The simulated concentrations at this station is strongly
371 underestimated with both the downscaled simulation at 0.004° (concentration
372 around 0.35 ng/m^3) and the coarse simulation (concentration around 0.26 ng/m^3).
373 Difficulties to reproduce exactly the spatiotemporal distribution of application
374 may explain the differences between the model and measurements.

375 With the exclusion of this station, a better spatial correlation was obtained
376 with the coarse simulation (0.75) than with the downscaled simulation (0.65).
377 However, these differences in the correlation is probably not statistically signif-
378 icant. On the 16 stations with measurements during the period of simulation,
379 results were improved for 5 stations (relative error decreased by 16% to 67%)
380 and degraded for 7 stations (relative error increased by 11% to 38%). Due to low
381 number of stations and the poor temporal coverage, it is therefore difficult to
382 evaluate the gain of performance due to the downscaling approach. Moreover,
383 errors due to the spatiotemporal distribution of applications in the vicinity of
384 the station probably increases with the resolution. Valari and Menut (2008) has
385 indeed shown that model results do not improve monotonously with resolution
386 and that after a certain point discrepancies with measurements become larger
387 due to insufficient precision in input data.

388 4. Conclusions

389 A downscaling method have been developed and applied on the simulation
390 of high resolution concentrations of S-metolachlor. The developed downscaling
391 method performs reasonably well (MNE around 7.9%) and can be used to sim-
392 ulate the hotspots of pesticide concentrations. The method developed in this
393 study is an important step toward high-resolution CTM simulations and the use
394 of CTM simulation for epidemiological studies on pesticides.

395 The current methodology does not account for spray-drift droplets as the
396 lifetime of these droplets can be considered too low compared to the resolution
397 of the model. One possible solution could be to implement plume-in-grid ap-
398 proaches (Karamchandani et al., 2006), in which a subgrid-scale representation
399 of plumes is embedded into CTMs. Other models aiming at representing the
400 local transport of spray-drift in the vicinity of the crops could also be used
401 (Raupach et al., 2001; Tsai et al., 2005; Zhang et al., 2018).

402 Acknowledgements

403 This work has been carried out thanks to the support of the COPP'R project
404 funded by the PRIMEQUAL – AGRIQA “Agriculture et qualité de l’air” and
405 the ECOPHYTO programs. We would like to thank all the participants of
406 the project for the useful discussions: Sophie Vannier (Vaucluse Chamber of
407 Agriculture). We thank the other member of BNVD-S Team for providing the
408 database and for the necessary discussions: Rémy Ballot, Corentin Barbu, Eric
409 Cahuzac (INRAE), Christophe Lescot, Laure Malherbe (INERIS). We especially
410 thank Eric Cahuzac who lead the BNVD-S project at the start of our work on
411 the modeling of pesticides. Simulations were performed using the TGCC-CCRT
412 supercomputers under the GENCI time allocation gen7485.

413 References

- 414 AtmoFrance, 2019. Base de donnée de surveillance de
415 pesticides dans l'air par les aasqa à partir de 2002.
416 <https://atmo-france.org/wp-content/uploads/2021/02/PhytAtmo>
417 [-donnees-pesticides_2002_2019.xlsx](#). Accessed: 2021-03-24.
- 418 Bessagnet, B., Pisoni, E., de Meij, A., Létinois, L., Thunis, P., 2023. A simple
419 and fast method to downscale chemistry transport model output fields from
420 the regional to the urban/district scale. *Environ. Model Softw.* 164, 105692.
421 doi:10.1016/j.envsoft.2023.105692.
- 422 Cognez, N., Warembourg, C., Zaros, C., Metten, M., Bouvier, G., Garlantézec,
423 R., Charles, M., Béranger, R., Chevrier, C., 2019. Residential sources of
424 pesticide exposure during pregnancy and the risks of hypospadias and cryp-
425 torchidism: the french elfe birth cohort. *Occup. Environ. Med.* 76, 672–679.
426 doi:10.1136/oemed-2019-105801.
- 427 Coscollà, C., López, A., Yahyaoui, A., Colin, P., Robin, C., Poinsignon, Q.,
428 Yusà, V., 2017. Human exposure and risk assessment to airborne pesti-
429 cides in a rural french community. *Sci. Total Environ.* 584-585, 856 – 868.
430 doi:10.1016/j.scitotenv.2017.01.132.
- 431 Couvidat, F., Bedos, C., Gagnaire, N., Carra, M., Ruelle, B., Martin, P.,
432 Poméon, T., Alletto, L., Armengaud, A., Quivet, E., 2022. Simulating the
433 impact of volatilization on atmospheric concentrations of pesticides with the
434 3d chemistry-transport model chimere: Method development and application
435 to s-metolachlor and folpet. *Journal of Hazardous Materials* 424, 127497.
436 doi:10.1016/j.jhazmat.2021.127497.
- 437 Couvidat, F., Bessagnet, B., 2021. Role of ecosystem-atmosphere exchanges of
438 semi-volatile organic compounds in organic aerosol formation. *Atmos. Envi-*
439 *ron.* , 118541doi:10.1016/j.atmosenv.2021.118541.
- 440 Couvidat, F., Sartelet, K., 2015. The secondary organic aerosol processor
441 (SOAP v1.0) model: a unified model with different ranges of complexity
442 based on the molecular surrogate approach. *Geosci. Model Dev.* 8, 1111–
443 1138. doi:10.5194/gmd-8-1111-2015.
- 444 Denby, B.R., Gauss, M., Wind, P., Mu, Q., Grøtting Wærsted, E., Fagerli, H.,
445 Valdebenito, A., Klein, H., 2020. Description of the uemep_v5 downscaling
446 approach for the emep msc-w chemistry transport model. *Geosci. Model Dev.*
447 13, 6303–6323. doi:10.5194/gmd-13-6303-2020.
- 448 Désert, M., Ravier, S., Gille, G., Quinapallo, A., Armengaud, A., Pochet,
449 G., Savelli, J.L., Wortham, H., Quivet, E., 2018. Spatial and tempo-
450 ral distribution of current-use pesticides in ambient air of provence-alpes-
451 côte-d'azur region and corsica, france. *Atmos. Environ.* 192, 241 – 256.
452 doi:10.1016/j.atmosenv.2018.08.054.
- 453 Hooyberghs, H., De Craemer, S., Lefebvre, W., Vranckx, S., Maiheu, B.,
454 Trimpeneers, E., Vanpoucke, C., Janssen, S., Meysman, F., Fierens, F., 2022.
455 Validation and optimization of the atmo-street air quality model chain by

- 456 means of a large-scale citizen-science dataset. *Atmos. Environ.* 272, 118946.
457 doi:10.1016/j.atmosenv.2022.118946.
- 458 Hough, I., Sarafian, R., Shtein, A., Zhou, B., Lepeule, J., Kloog, I.,
459 2021. Gaussian markov random fields improve ensemble predictions of
460 daily 1 km pm2.5 and pm10 across france. *Atmos. Environ.* 264, 118693.
461 doi:https://doi.org/10.1016/j.atmosenv.2021.118693.
- 462 Karamchandani, P., Vijayaraghavan, K., Chen, S.Y., Seigneur, C., Edgerton,
463 E.S., 2006. Plume-in-grid modeling for particulate matter. *Atmos. Environ.*
464 40, 7280–7297. doi:10.1016/j.atmosenv.2006.06.033.
- 465 Letinois, L., 2015. Méthodologie de répartition spatiale de la population. Tech-
466 nical Report. LCSQA, Laboratoire central de surveillance de la qualité de
467 l’air, France.
- 468 Lichiheb, N., Personne, E., Bedos, C., Van den Berg, F., Barriuso, E.,
469 2016. Implementation of the effects of physicochemical properties on
470 the foliar penetration of pesticides and its potential for estimating pes-
471 ticide volatilization from plants. *Sci. Total Environ.* 550, 1022–1031.
472 doi:10.1016/j.scitotenv.2016.01.058.
- 473 Mailler, S., Menut, L., Khvorostyanov, D., Valari, M., Couvidat, F., Siour, G.,
474 Turquety, S., Briant, R., Tuccella, P., Bessagnet, B., Colette, A., Létinois,
475 L., Markakis, K., Meleux, F., 2017. CHIMERE-2017: from urban to hemi-
476 spheric chemistry-transport modeling. *Geosci. Model Dev.* 10, 2397–2423.
477 doi:10.5194/gmd-10-2397-2017.
- 478 Martin, P., Ramalanjaona, L., Truche, C., Ballot, R., Carozzi, M., Pomeon,
479 T., 2023. Modelling the spatialisation of pesticide sales to monitor envi-
480 ronmental policies in france. *Journal of Cleaner Production* 403, 136880.
481 doi:10.1016/j.jclepro.2023.136880.
- 482 Moussaoui, Y., Tuduri, L., Kerchich, Y., Meklati, B., Eppe, G., 2012. At-
483 mospheric concentrations of pcdd/fs, dl-pcbs and some pesticides in north-
484 ern algeria using passive air sampling. *Chemosphere* 88, 270 – 277.
485 doi:10.1016/j.chemosphere.2012.02.025.
- 486 Raupach, M., Briggs, P., Ahmad, N., Edge, V., 2001. Endosulfan transport: Ii.
487 modeling airborne dispersal and deposition by spray and vapor. *J. Environ.*
488 *Qual.* 30, 729–740. doi:10.2134/jeq2001.303729x.
- 489 Shen, Y., de Hoogh, K., Schmitz, O., Clinton, N., Tuxen-Bettman, K., Brandt,
490 J., Christensen, J.H., Frohn, L.M., Geels, C., Karssenber, D., Vermeulen, R.,
491 Hoek, G., 2022. Europe-wide air pollution modeling from 2000 to 2019 using
492 geographically weighted regression. *Environment International* 168, 107485.
493 doi:10.1016/j.envint.2022.107485.
- 494 Teyssere, R., Manangama, G., Baldi, I., Carles, C., Brochard, P., Bedos, C.,
495 Delva, F., 2020. Assessment of residential exposures to agricultural pesticides:
496 A scoping review. *PLOS ONE* 15, 1–19. doi:10.1371/journal.pone.0232258.

- 497 Tsai, M.Y., Elgethun, K., Ramaprasad, J., Yost, M.G., Felsot, A.S., Hebert,
498 V.R., Fenske, R.A., 2005. The washington aerial spray drift study: Modeling
499 pesticide spray drift deposition from an aerial application. *Atmos. Environ.*
500 39, 6194 – 6203. doi:10.1016/j.atmosenv.2005.07.011.
- 501 Valari, M., Menut, L., 2008. Does an increase in air quality models' resolu-
502 tion bring surface ozone concentrations closer to reality? *J. Atmos. Ocean.*
503 *Technol.* 25, 1955 – 1968. doi:10.1175/2008JTECHA1123.1.
- 504 Vestreng, V., 2003. Review and revision. Emission data re-
505 ported to CLRTAP Tech. Rep., EMEP MSW-W. Technical Re-
506 port. Norwegian Meteorological Institute, Oslo, Norway. URL:
507 https://emep.int/publ/reports/2003/mscw_note_1_2003.pdf.
- 508 Zhang, X., Luo, Y., Goh, K.S., 2018. Modeling spray drift and runoff-related
509 inputs of pesticides to receiving water. *Environ. Pollut.* 234, 48 – 58.
510 doi:10.1016/j.envpol.2017.11.032.